Multiple spatial spectral components of static skin deformation for predicting macroscopic roughness perception

Qingyu Sun[1], Shogo Okamoto[1,2], Yasuhiro Akiyama[3], and Yoji Yamada[1,4]

***Abstract*—A previous study suggested a relationship between the spatial spectrum of finger pad skin deformation and perception of macroscopic roughness features. This study tested a new hypothesis that macroscopic roughness perception is the result of a weighted linear combination of multiple spatial spectral components of skin deformation. Experiments were conducted by capturing close-up images of finger pad deformation while the pads were pushed onto specimens with macroscopic features. Additionally, the roughness perceptions of these specimens were collected using a magnitude estimation method. The combination of spectral components predicted the roughness perception more accurately than any single spectral component. This suggests that roughness perception is mediated by multiple Gabor filter-like neural systems with different spatial periods, such as visual perception.**

I. Introduction

Roughness is a fundamental property of texture perception [1]–[3]. Many neurophysiological and psychophysical studies have elucidated the perceptual mechanisms of this property. For example, neurophysiological studies have found that slowly adapting type-I (SAI) units play a significant role in perceiving macroscopic surface roughness [4]–[6]. SAI units are responsible for sustained skin deformation and pressure [7], and their neural activity can be a function of local stress in the skin [8], [9]. In contrast, fast-adapting units mediate microscopic roughness features [10]–[12]. These units are sensitive to skin vibrations caused when the finger slides over textured surfaces. In psychophysics, the relationship between surface features and roughness perception has been extensively studied. For example, the inter-dot spaces of dot scales and groove widths of grating scales are considered the primary determinants of the perceived roughness [13]–[17]. Humans typically feel the most intense roughness for grating scales with groove widths in the range of 2.0 to 4.0 mm [11], [14], [15], [18]–[20].

Thus far, neurophysiological studies have mainly focused on how afferent units respond to roughness features and skin deformation [4]–[6], [9], [21], [22]. Psychophysical studies have primarily focused on the dependence of roughness perception on roughness features [13]–[17], [23]. Although roughness perception, skin deformation, and afferent activation occur after touching rough surfaces, few studies have attempted to link skin deformation and perceived roughness when touching rough surfaces. For example, Taylor and Ledermann proposed that the penetration of the finger pad skin into the grooves could be the determinant of the perception of macroscopic roughness [24]. Okamoto and Oishi pointed out that the spatial spectral components of the surface deformation of finger skin are highly correlated with the roughness perception of macroscopic grating scales [25].

In [25], the authors predicted the perceived roughness using a single spatial spectral component of the finger pad deformation and the outputs of a single Gabor filter, which is a classical basis function for wavelet transform. They found that components with wavelengths ranging from 2.45 to 4.00 mm exhibited high correlation with subjective roughness. These wavelength values are close to those used in neurophysiological studies [11], [18], [26], where roughness perception was estimated based on Gabor-filter outputs of spatial neural activation plots of SAI units. These studies [18], [25]–[27] considered the existence of an optimal wavelength for the Gabor filter and an optimal spatial frequency for estimating macroscopic roughness perception. Tymms et al. estimated the roughness perception based on the simulated spatial variation of compressive strains in an elastic model pressed on roughened surfaces and found that the optimal spatial distance for computing the spatial variation was smaller than 2.4 mm [28][1]. In other words, they hypothesized that there is only one type of Gabor-filter-like neural detector for SAI activity that is responsible for macroscopic roughness.

This study focused on the question of whether there may be multiple types of detectors with different sensitive wavelengths and how the linear combination of these detector outputs may contribute to roughness perception. This is a natural expansion from simple cells to complex cells in the primary visual cortex, where a simple cell functions as a Gabor filter, and different simple cells exhibit sensitivities to different spatial wavelengths. The combination of these simple cells innervates other neural cells for complex processing of visual information [29].

We captured close-up images of the finger pad deformation while pushing the pads against grating scales with macroscopic features. Gabor filters of various wavelengths were applied to the images of surface deformation of the skin to compute the spatial spectrum. The subjective roughness values for the grating scales were then measured using magnitude estimation. We established two types of estimators for the subjective roughness. The first estimator uses a single Gabor-filter output that responds intensely to a specific wavelength value. The second estimator uses a weighted linear combination of the outputs of multiple Gabor filters with different wavelengths. These two types of estimators were compared in terms of their estimation accuracy. If the latter estimator outperforms the former, it suggests that multiple types of Gabor filter-like detectors with sensitivities to different wavelengths exist. If the performance of these two types of estimators are comparable, it suggests that only one type of Gabor-filter-like detector is sensitive to a specific spatial wavelength function for macroscopic roughness perception.

This study extends the study conducted in [25] where the relationships between the spatial spectral components of static skin deformation and macroscopic-roughness perception were investigated. They

[1]Sun, Okamoto, and Yamada are with the Department of Mechanical Systems Engineering, Nagoya University, Nagoya, Aichi, Japan.

[2]Okamoto is also with the Department of Computer Science, Tokyo Metropolitan University, Hino, Tokyo, Japan. okamotos@tmu.ac.jp

[3]Akiyama is with the Department of Mechanical Engineering and Robotics, Shinshu University, Ueda, Nagano, Japan.

[4]Yamada is also with the National Institute of Technology, Toyota College, Toyota, Aichi, Japan.

This research was funded by MEXT Kakenhi 20H04263 and 21H05819. QS and SO are equal contributors.

[1]They computed the variation of strains between two separate circular regions instead of points. Hence, their definition of distance is different from those in other studies.

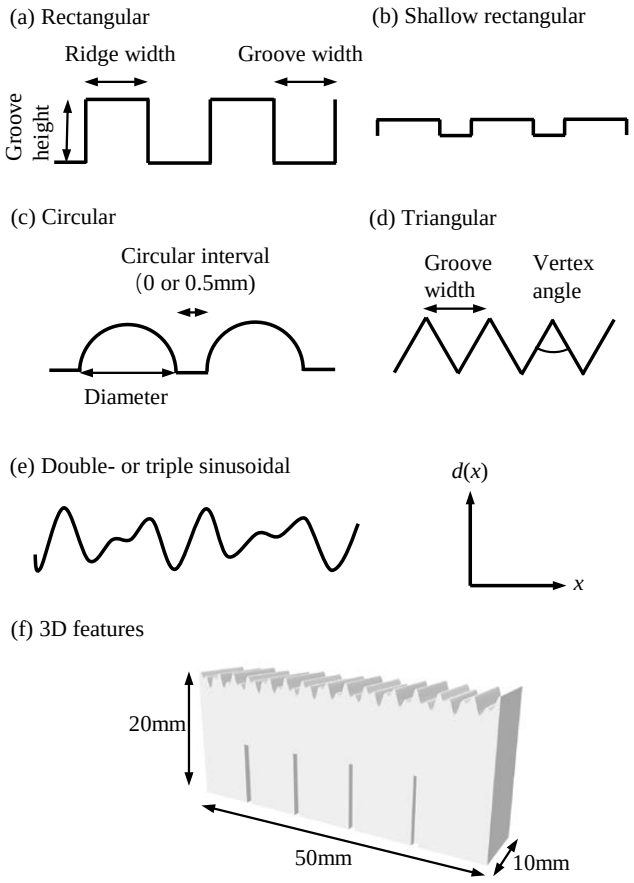

Fig. 1. Five types of grating scales: (a) rectangular, (b) shallow rectangular, (c) circular, (d) triangular, and (e) double- or triple-sinusoidal surfaces. (f) 3D view of grating scales.

concluded that the spectral components with wavelengths ranging 2.45–4.00 mm nearly equally predicted roughness perception. To determine which component best predicts roughness perception, they used rectangular, circular, and triangular roughness grating scales in their experiment. By contrast, we investigated the effect of combining multiple components, for which more complex roughness scales must be adopted. Roughness scales with two or three spatial frequency components were used in this study.

II. METHODOLOGY

The protocol for this experiment was approved by the Institutional Review Board of the School of Engineering, Nagoya University (#19-9).

A. Grating roughness scales

Six types of 3D-printed grating scales were used: rectangular, shallow rectangular, triangular, circular, double-sinusoidal, and triple-sinusoidal, as shown in Fig. 1. The printer was Form 3 (Formlabs, MA) with a nominal resolution of 25 μm. After printing the specimens, we visually and haptically inspected their surfaces and verified that they had no recognizable microscopic patterns. The dimensions of the specimens were 50 $\times$ 20 $\times$ 10 mm. The rectangular specimens were defined by the groove and ridge widths, whereas the shallow rectangular specimens also included the groove height. The groove height of the shallow rectangular specimens was designed so that the finger skin would reach the bottom of the grooves. Shallow and deep grating scales lead to different roughness perceptions, even if they have the same groove width and ridge width. Shallow macroscopic-roughness specimens elicit a smaller roughness perception than deep specimens [30]. Hence, we included both deep and shallow rectangular scales to investigate the contribution of the magnitude of skin deformation. Triangular specimens were defined based on the vertex angle and groove width. Circular specimens were defined by their diameters and intervals between two neighboring semicircular shapes. To extend our experiment to a wider variety of surfaces, we introduced double- and triple-sinusoidal specimens. The surfaces of the triple-sinusoidal specimens were defined by the sum of three sinusoidal functions as follows:

$$d(x) = a_1 \sin(2\pi \frac{x}{\lambda_1}) + a_2 \sin(2\pi \frac{x}{\lambda_2}) + a_3 \sin(2\pi \frac{x}{\lambda_3}), \quad (1)$$

where $a_{1,2,3}$ and $\lambda_{1,2,3}$ denote the amplitude and spatial wavelength, respectively, in millimeters. The double-sinusoidal specimens were defined by the first two sinusoidal functions. Two or three sinusoidal components were superimposed with no phase differences. The λ values were chosen such that they differed by at least 0.5 mm and were not multiples of each other. Furthermore, we adjusted the amplitudes such that the double- and triple-sinusoidal specimens are approximately divided into two groups. In one group, the finger pads could reach the bottom of the grooves, whereas in the other group they could not. Some specimens were excluded because they had large peak heights and the finger pads could not contact the surfaces in multiple separated areas.

These shapes, excluding the double- and triple-sinusoidal and shallow rectangular scales, were also used in [25]. Although most previous psychophysical studies adopted only a single type of scales [14]–[17], [26], we used all six types of grating scales mentioned above. We originally designed over 60 different specimens and then excluded those with similar subjective roughness perceptions while maintaining a variety of shapes. The specific parameters of the 37 specimens used are listed in Table I.

B. Participants

Ten university students (22 $\pm$ 2.0 (mean and standard deviation) years) participated in this experiment after providing written informed consent. The objectives of this study were not explained to the participants before the experiments.

C. Magnitude estimation of roughness perception

Magnitude estimation tasks were conducted to measure participants' subjective roughness perceptions of the specimens. A circular grating scale with a diameter of 2 mm and groove width of 0.25 mm was used as the modulus with a roughness value of 100. All the specimens were rated relative to the modulus (i.e., if the roughness of one specimen was perceived to be three times that of the modulus, its roughness perception was 300). The participants were required to place their index finger parallel to the specimen and push it with a force of 300 gf according to an electric scale. This pressing force, i.e., 300 gf, lies in the range of the values at which roughness perception functions fairly [31]. Fig. 2 shows the variations in pressing force in typical trials. The participants identified the roughness magnitudes after removing their fingers from the stimulus. No sliding motion was allowed on the specimens. Each specimen was tested three times, and the specimens were presented in random order. A total of 111 trials (37 specimens $\times$ three repetitions) were conducted in randomized order for each participant. The participants wore a pair of glasses whose lenses were blurred by translucent tape, so that they could not see the detailed shapes of the specimens.

TABLE I
PHYSICAL PARAMETERS OF 37 GRATING SCALES

	Ridge width (mm)	Groove width (mm)	Vertex angle (°)	Circular diameter (mm)	Groove height (mm)	Symbol
Rectangular	0.75	1.0	-	-	3.0	a
	0.75	1.75	-	-	3.0	b
	1.0	1.0	-	-	3.0	c
	1.0	2.25	-	-	3.0	d
	1.5	1.5	-	-	3.0	e
Shallow rectangular	1.0	2.25	-	-	0.25	f
	1.0	2.25	-	-	0.5	g
	0.75	1.0	-	-	0.25	h
	0.75	1.75	-	-	0.25	i
Triangular	0	1.0	30	-	-	j
	0	1.5	30	-	-	k
	0	1.75	30	-	-	l
	0	2.75	45	-	-	m
	0	4.0	60	-	-	n
Circular	0	0	-	1.0	-	o
	0	0.5	-	1.75	-	p
	0	0	-	2.5	-	q
	0	0	-	3.0	-	r
	0	0	-	4.0	-	s

	a_1 (mm)	a_2 (mm)	a_3 (mm)	λ_1 (mm)	λ_2 (mm)	λ_3 (mm)	Symbol
Double-sin	0.2	0.25		1.5	3.5		t
	0.2	0.4		1.5	2		u
	1	1		2	3		v
	0.05	0.15		1.5	2.5		w
	0.15	0.35		1.3	2.1		x
	0.35	0.2		1	1.7		y
	0.3	0.2		1.7	3.8		z
Triple-sin	0.1	0.3	0.2	1	1.6	2.2	1
	0.1	0.2	0.15	1.2	2.7	4.3	2
	0.1	0.25	0.2	1.6	2.3	3.1	3
	0.2	0.2	0.2	1	1.6	3.3	4
	0.2	0.15	0.25	1.1	2.7	3.4	5
	0.2	0.25	0.2	1.3	2.1	3.1	6
	0.15	0.2	0.1	1.3	2.4	3.1	7
	0.15	0.1	0.15	1.6	2.4	3.9	8
	0.3	0.4	0.2	1.2	1.8	2.9	9
	0.15	0.35	0.4	1.3	1.9	3.4	10
	0.25	0.4	0.3	1.2	1.7	2.8	11

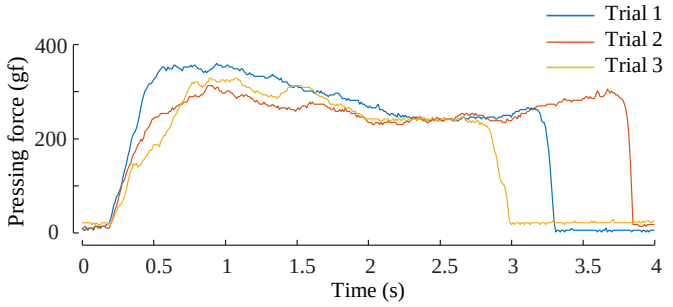

Fig. 2. Example profiles of normal force during magnitude estimation trial. Profiles of the three trials are shown.

For our subsequent analysis, we used the median values of three trials for each roughness scale. The values were then shifted such that the mean was zero for each individual according to the computational requirements described in Section II-F.

D. Skin images and spatial spectra

Similar to the magnitude estimation task, participants placed their index fingers parallel to the specimens and applied a normal force of 300 gf. A cross-sectional image was captured using a digital camera

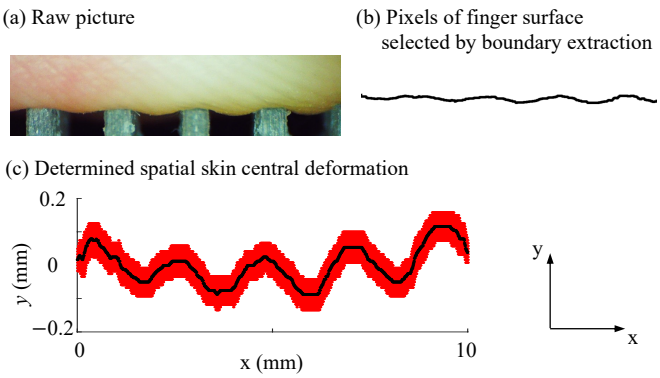

Fig. 3. (a) Original image of an index finger captured from the lateral side. (b) Extracted finger deformation region. (c) Central curve (black) of surface deformation region (red).

(3R-Viewter-500uv, 3R Solution Ltd., Japan; 500 million pixels) as shown in Fig. 3a. The deformation curve of the skin surface was obtained using Photoshop (ver. 2019, Adobe Inc., CA), in which the *quick selection tool* and *stroke* functions were used to select the skin border, as shown in Fig. 3b. The camera zoom was adjusted such that the image resolution was 1200 pixels/cm. As shown in Fig. 3c, the binarized images were processed using MATLAB (MATLAB, 2021a, Mathworks, MA, USA). The red area represents the region extracted by the aforementioned process after removing the linear trend. The central curve of this region was used to represent the surface deformation of the skin.

We used a one-dimensional Gabor filter to compute the spatial spectra from the processed curves of finger deformation. As shown in Fig. 4a, the one-dimensional Gabor filter is a combination of a cosine function with a spatial period (λ mm) and exponential attenuation.

$$g(x) = \exp(\frac{-x^2}{2\sigma^2})\cos(\frac{2\pi x}{\lambda}), \tag{2}$$

where σ denotes the width of the amplitude attenuation and λ^{-1} denotes the central spatial frequency. σ was set to 1.1 mm as described in [25], [26], [32]. Fig. 4b shows the extracted central deformation of the skin, that is, the black border line in Fig. 3c. As shown in Fig. 4c, for each λ value, the convolution was computed between the Gabor filter and deformation curve as follows:

$$g_o(x) = (g * y)(x) \tag{3}$$

where $y(x)$ is the skin displacement in mm normal to the contact surface at position x. The maximum absolute output of the Gabor filter is used as the value of the spatial spectral component for λ.

As shown in Fig. 4d, the spatial spectrum $s(\lambda)$ is the set of spatial spectral components for different λ values computed from a single image of skin deformation. We vary the parameter λ from 0.35 to 4.95 mm with an interval of 0.2 mm. There may be no clear boundary between microscopic and macroscopic roughness, although most researchers agree that the mechanism for roughness perception changes below or above the spatial wavelength ranging from hundreds of μm to 1 mm [14], [33], [34]. Although we used the range of 0.35–4.95 mm, a slight variation did not affect our final conclusions. For example, the adoption of a range of 0.10–6.9 mm did not improve the final estimation accuracy of the subjective roughness.

E. Weight function for the spatial spectra used to predict subjective roughness

In continuous form, the subjective roughness value r is hypothesized to be the integral of the weight function $w(\lambda)$ and spatial

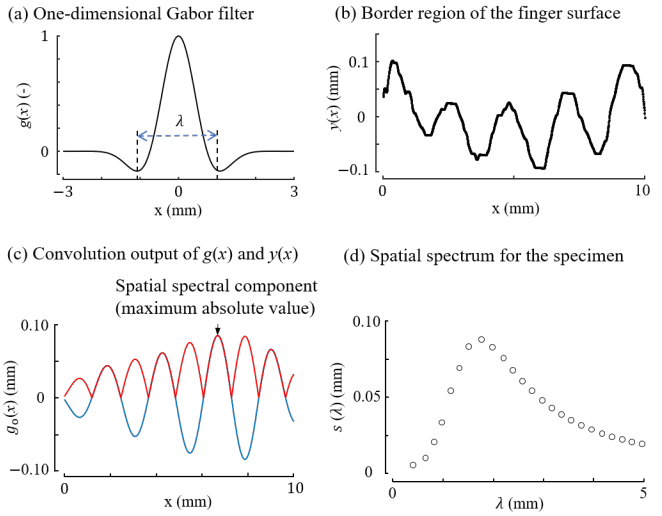

Fig. 4. Computation of a spatial spectrum. (a) One-dimensional Gabor filter with spatial period λ. (b) Skin deformation curve $y(x)$. (c) Convolution output between $g(x)$ and $y(x)$ (in blue). The maximum absolute value (red) is the spatial spectral component of the spatial period λ. (d) Spatial spectrum computed from an image of skin deformation for λ values ranging from 0.35 to 4.95 mm.

spectrum $s(\lambda)$, as follows:

$$r = \int_{0.35}^{4.95} s(\lambda) w(\lambda)\, d\lambda. \tag{4}$$

In the discrete form, r is computed from the inner product of the spatial spectrum vector $\boldsymbol{s} \in \mathbb{R}^{24\times 1}$ containing 24 spectral components for λ ranging from 0.35–4.95 mm with increments of 0.20 mm and the perceptual weight $\boldsymbol{w} \in \mathbb{R}^{24\times 1}$, as follows:

$$r = \boldsymbol{s}^{\mathrm{T}} \boldsymbol{w}. \tag{5}$$

This formula holds for all trials, that is, all combinations of specimens and participants, as follows:

$$\begin{pmatrix} r_1 \\ \vdots \\ r_n \end{pmatrix} = \begin{pmatrix} \boldsymbol{s}_1^{\mathrm{T}} \\ \vdots \\ \boldsymbol{s}_n^{\mathrm{T}} \end{pmatrix} \boldsymbol{w}, \tag{6}$$

where n indicates the number of trials, and $\boldsymbol{s}_i$ $(i = 1, ..., n)$ denotes the spatial spectrum vector for the trial i. For all trials, (6) can be rewritten as follows:

$$\boldsymbol{r} = \boldsymbol{S}\boldsymbol{w}, \tag{7}$$

where $\boldsymbol{r} \in \mathbb{R}^{n\times 1}$ and $\boldsymbol{S} \in \mathbb{R}^{n\times 24}$ represent the vector of subjective roughness and the matrix of spatial spectra, respectively. The spectral components were normalized (z-scored) for individual participants and λ values. Owing to this normalization, $\boldsymbol{s}$ is dimensionless. Accordingly, $\boldsymbol{w}$ is also dimensionless. This process is necessary because the magnitude of skin deformation varies among individuals owing to the differences in skin hardness.

F. Computation of the weight function via partial least-squares regression

To solve for $\boldsymbol{w}$ in (7), a multiple regression approach is typically adopted and $\boldsymbol{w}$ is computed as

$$\boldsymbol{w} = \boldsymbol{S}^{+}\boldsymbol{r}, \tag{8}$$

where $\boldsymbol{S}^{+}$ is the generalized inverse matrix of $\boldsymbol{S}$. However, due to collinearity among the explanatory variables (i.e., spectral components), we employed another approach known as partial least-squares (PLS) regression. PLS is a combination of multiple regression analyses and supervised principal component analysis (PCA). PLS uses the scores of the principal components (PCs) as explanatory variables that are correlated with objective variables (i.e., subjective roughness values). The PCs are independent of each other; thus, the problem of collinearity can be circumvented.

Therefore, the computational method of PLS regression was adopted in this study. The matrix of spatial spectra $\boldsymbol{S}$ and the vector of subjective roughness $\boldsymbol{r}$ are decomposed into the scores of the u PCs as follows:

$$\boldsymbol{S} = \sum_{i=1}^{u} \boldsymbol{t}_i \boldsymbol{p}_i^{\mathrm{T}} + \boldsymbol{E} \tag{9}$$

$$\boldsymbol{r} = \sum_{i=1}^{u} a_i \boldsymbol{t}_i + \boldsymbol{e}, \tag{10}$$

where $\boldsymbol{t}_i \in \mathbb{R}^{n\times 1}$ denotes the score of the ith $(i = 1, ..., u)$ PC $\boldsymbol{p}_i \in \mathbb{R}^{24\times 1}$, and $\boldsymbol{E}$ and $\boldsymbol{e}$ denote the model errors. The number of PCs, denoted by u, was selected to maximize the prediction accuracy in a cross-validation method, as discussed in Section III. a_i is the coefficient of $\boldsymbol{t}_i$. Note that $\boldsymbol{t}_i \perp \boldsymbol{t}_j$ $(i \neq j)$ and collinearity are not a concern in (10).

In contrast to PCA, PLS regression analysis, determines the PCs $\boldsymbol{p}_i$ and their scores $\boldsymbol{t}_i$ in a supervised manner using the objective variable r. $\boldsymbol{t}_i$ is computed such that the covariance with $\boldsymbol{r}_i$ is maximized as follows:

$$\boldsymbol{t}_i = \frac{\boldsymbol{S}_i \boldsymbol{S}_i^{\mathrm{T}} \boldsymbol{r}_i}{\| \boldsymbol{S}_i^{\mathrm{T}} \boldsymbol{r}_i \|}, \tag{11}$$

where $\| \ \|$ denotes the L2 norm. Then, as least-squares solutions, $\boldsymbol{p}_i$ and a_i are computed as follows:

$$\boldsymbol{p}_i = \frac{\boldsymbol{S}_i^{\mathrm{T}} \boldsymbol{t}_i}{\| \boldsymbol{t}_i \|} \tag{12}$$

$$a_i = \frac{\boldsymbol{r}_i^{\mathrm{T}} \boldsymbol{t}_i}{\| \boldsymbol{t}_i \|}, \tag{13}$$

where $\boldsymbol{S}_1 = \boldsymbol{S}$ and $\boldsymbol{r}_1 = \boldsymbol{r}$. $\boldsymbol{S}_i$ and $\boldsymbol{r}_i$ are the explanatory and objective values, respectively, after excluding the influence of the PCs up to the $i-1$th component:

$$\boldsymbol{S}_i = \boldsymbol{S}_{i-1} - \boldsymbol{t}_{i-1} \boldsymbol{p}_{i-1}^{\mathrm{T}} \tag{14}$$

$$\boldsymbol{r}_i = \boldsymbol{r}_{i-1} - a_{i-1} \boldsymbol{t}_{i-1}. \tag{15}$$

Using the coefficients a and PC vectors $\boldsymbol{p}$, we calculate the weighting vector $\boldsymbol{w}$ as:

$$\boldsymbol{w} = \sum_{i}^{u} a_i \boldsymbol{p}_i. \tag{16}$$

III. Results

A leave-one-out cross-validation method was used to determine the number of PCs for PLS regression. For this computation, all participants, except for one who was used as the testing dataset, were used as the training dataset. The test participants were then switched to calculate the mean estimation performance of the regression models. R^2 was calculated for the estimation of subjective roughness using the PLS models, and it was the highest (0.636) when two PCs were used. The R^2 value was 0.630 when only the first PC was used. Therefore, we selected the first two PCs for PLS regression.

Fig. 5a presents the relationship between the reported and estimated subjective roughness values for all trials with ten participants when

(a) Subjective roughness & estimated subjective roughness by a weighted spatial spectrum

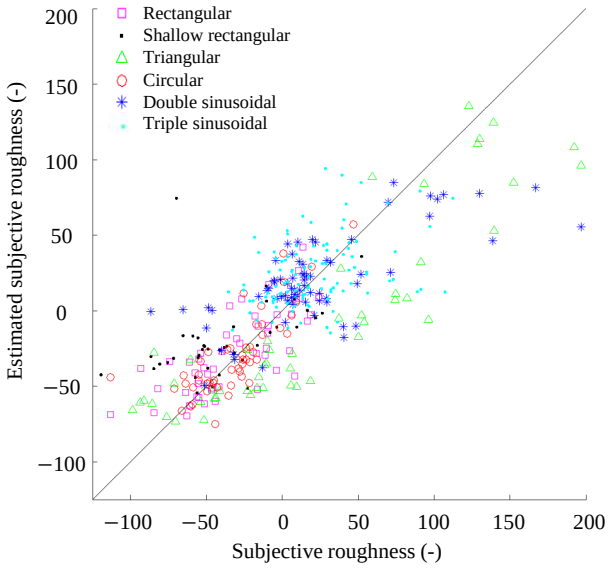

(b) Mean reported & estimated subjective roughness among participants by PLS regression

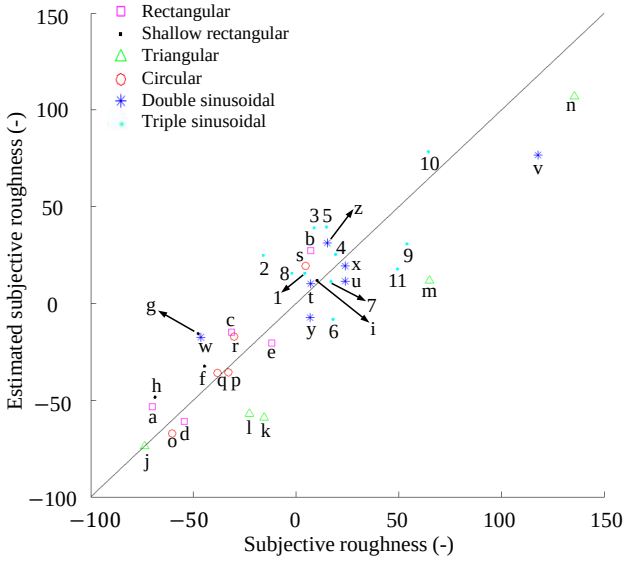

Fig. 5. Estimation of subjective roughness. (a) Reports and estimates using PLS regression. (b) Mean reports and estimates among the participants using PLS regression.

the first two PCs were incorporated into the weighted linear model. The correlation coefficient was 0.78 (R^2 is 0.61). Table II lists the mean absolute errors (MAE) of the two estimators, i.e., single spatial spectral component and weighted spatial spectrum. The participants' subjective roughness ranged from approximately -100 to 200, and the overall MAE was 27.77 and 23.53 for the single spatial component and weighted spatial spectrum, respectively. The weighted spatial spectrum exhibited smaller estimation errors, particularly for the rectangular, circular, and triple-sinusoidal specimens.

The average correlation coefficient between the reported and estimated subjective roughness values was 0.82 ± 0.023 (mean and standard error), with maximum and minimum values of 0.91 and 0.69, respectively, when the model was executed for individuals.

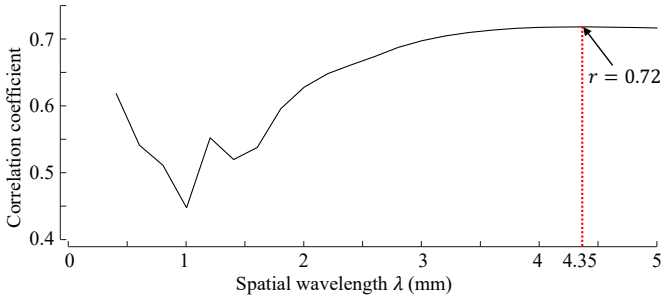

Fig. 6. Correlation coefficients between single spatial components and reported subjective roughness.

TABLE II
MEAN ABSOLUTE ERROR (MAE) OF THE TWO ESTIMATORS BASED ON DIFFERENT SURFACE SHAPES

Type	MAE by a single spatial spectral component	MAE by weighted spatial spectrum
Rectangular	22.76	17.46
Shallow rectangular	26.74	26.08
Triangular	40.38	37.24
Circular	22.47	12.62
Double-sinusoidal	26.02	24.84
Triple-sinusoidal	28.23	23.26
Mean	27.77	23.53

Fig. 5b presents the estimation performance of PLS regression after averaging the individual responses. The correlation coefficient was 0.88. The triangular specimens tended to be underestimated except for those with a groove width of 1 mm (denoted as 'j'). In contrast, the predictions for rectangular and circular specimens were relatively accurate. The estimations for double-sin and triple-sin specimens were also fairly accurate.

Fig. 6 shows the variation in correlation coefficients between the single spatial spectral component and subjective roughness, which generally increases to 0.72 at $\lambda = 4.35$ mm, although there is a local peak at 1.15 mm.

We compared the spatial spectrum weighted by the two PCs and the single spatial spectral component at 4.35 mm in terms of the correlation coefficients between the reported and estimated subjective roughness. The correlation coefficients were calculated for individual participants and then normalized using the Fisher z-transformation among all participants. The correlation coefficients obtained using the weighted spatial spectrum ($r = 0.82 \pm 0.023$, mean $\pm$ standard error) were significantly higher than those obtained using the single spatial spectral component ($r = 0.75 \pm 0.023$)[2] with $t = -8.83$ and $p = 9.97 \times 10^{-6}$ by a paired t-test.

Even when only the first PC was used in the weighted spatial spectrum, the correlation coefficient between the reported and estimated subjective roughness was higher ($r = 0.80 \pm 0.027$) than that of the single spatial spectral component ($t = 5.23$, $p = 5.40 \times 10^{-4}$). Therefore, the first PC was sufficient for testing our hypothesis. We selected two PCs such that the R^2 was maximized through cross-validation, although the contribution of the second component was minor.

Fig. 7 presents the weight vector $\boldsymbol{w}$ for the spatial spectral components. As in (7), this links the subjective roughness with the spatial spectra of skin deformation. The peak value lies at $\lambda = 3.15$ mm, indicating that macroscopic roughness perception is most sensitive

[2]Note that 0.72 in Fig. 6 was calculated using all the samples of all participants, whereas 0.75 was the mean of the correlation coefficients among all individuals.

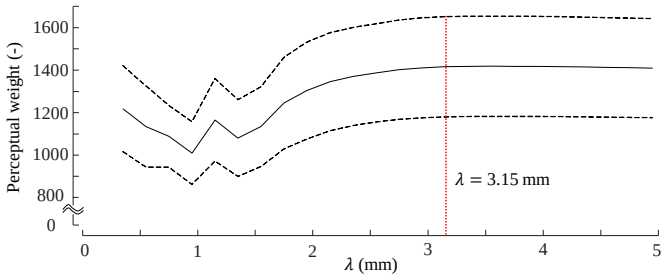

Fig. 7. Weight vector $\boldsymbol{w}$ acquired by PLS regression with 95% confidence interval. The confidence interval was computed by the variation of the weights among the participants.

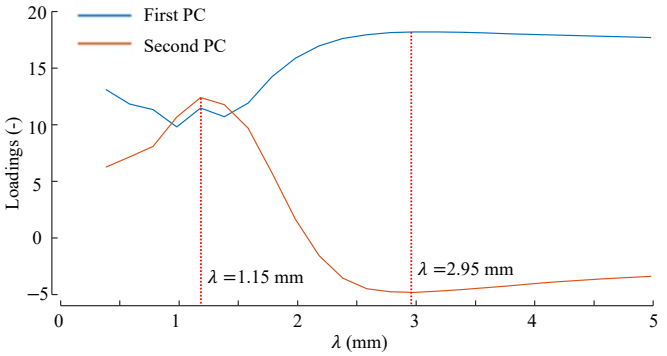

Fig. 8. Loading vectors $\boldsymbol{p}$ for the first two PCs obtained by PLS regression. The blue curve represents the first PC and the orange curve represents the second PC.

to a wavelength of 3.15 mm. However, considering the confidence interval, a true peak may exist approximately above 2.5 mm.

Fig. 8 shows the vectors $\boldsymbol{p}$ of the first two PCs obtained using PLS regression. The first PC shows a perceptual peak at 2.95 mm, while the second PC has a peak at 1.15 mm.

IV. Discussion

In this study, we used six types of grating scales, in contrast to previous studies that did not test specimens on different types of scales (e.g., [14], [15], [17], [26]). As shown in Fig. 5, the roughness perception for all types of grating scales can be estimated based on the finger pad skin deformation; however, triangular scales tend to be underestimated. A potential explanation for this is that the triangular specimens were not perceived purely as roughness stimuli. They also included pain stimuli owing to their pointed edges, although no participant complained of unacceptable pain during the experiments. In the magnitude estimation task, participants may have responded to roughness plus pain perception; thus, the reported values were greater than those obtained through pure roughness perception.

Although previous studies have considered the contribution of a single spatial spectral component to macroscopic roughness perception [18], [25]–[27], this study investigated the hypothesis that macroscopic roughness perception is mediated by a weighted linear combination of multiple spectral components. The single spatial component for $\lambda = 4.35$ mm exhibited a correlation coefficient of 0.75 ± 0.023 with the reported roughness values. This correlation coefficient was significantly lower than that for the linear combination of spectral components, which was 0.82 ± 0.023. These results suggest that humans utilize multiple Gabor filter-like detectors, such as those in the visual system.

This raises the question of what these two PCs indicate. As shown in Fig. 8, each of the two PCs exhibit a peak in a certain spatial period. The first PC has a peak at 2.95 mm. This value is close to the results of former studies (2.8 mm in [18], [26]). This value may be related to the activity of the SAI-unit system. The second PC exhibits a peak at 1.15 mm. This may be mediated by the fast adaptive (FA) units. In our experimental protocol, we asked the participants to press their fingertips on the specimens until the electronic scale showed a force of 300 gf; thus the fingers went through an active pushing process. Therefore, the subjective roughness reported in our experiment might have been due to the combined effect of SAI and FA activities, although FA units were observed as a relatively minor factor in our setting.

Here, we discuss the wavelength of the spatial component that is most sensitive to the roughness perception. It is reasonable to assume that such a wavelength is largely determined by the spatial distribution of SAI units beneath the skin. The density of the SAI units at the fingertip is approximately 70 units per cm^2 [35], [36]. Based on this density and the assumption that SAI units have equal spacing distances, we performed calculations and found that the average distance between two neighboring SAI fibers was approximately 1.45 mm. If each SAI unit is considered as a pressure-sensitive element, then based on the sampling theorem, the system of SAI units is suitable for detecting spatial wavelength components of 2.90 mm or greater. This value is close to those used for the wavelengths of the filters applied to the spatial activity plots of SAIs: 2.8 mm in [18], [26] and 2.6 mm in [11]. Furthermore, in [25], which is the basis of our study, the spatial spectral component of 2.66 mm exhibited the largest correlation coefficient with roughness perception. As shown in Fig. 7, the maximum perceptual weight was $\lambda = 3.15$ mm. These values considerably overlap with the loci of the maximum subjective roughness reported in [14], [15], [19], [37], where the roughness perception expressed as a function of the spatial periods of the grating scales and dot scales exhibited inverted U-shaped curves with maximum values at approximately 2.0–4.0 mm. In a study using the spatial spectra of finger pads [25], the spatial components between 2.45 to 4.00 mm exhibited equally high correlation coefficients for roughness perception. Furthermore, Connor et al. [18] reported that Gabor filters with $\lambda = 2.0$–4.0 mm exhibited equally good performance in estimating subjective roughness. The SAI units are not uniformly distributed beneath the skin, and each unit has several branches with several Merkel cells at their ends [21]. Additionally, the densities of the afferent units depend on finger size [38], [39]. Therefore, we cannot expect a unique optimal λ value. Instead, we speculate that the spatial spectral components for wavelengths of approximately 2.0 to 4.0 mm are equally sensitive to the perception of macroscopic roughness.

Previous studies have suggested that in the relationship between tactile acuity and finger size, small fingers lead to dense epidermal ridges and SAI units [38], [39]. Although individual finger sizes were not recorded in this study, if a correlation between finger size and the most significant λ value in the perceptual weight vector is identified, then we will have clues on how to determine the most suitable λ value for different individuals. Moreover, although the finger pressing force was controlled at approximately 300 gf in our study, humans do not strictly control their pressing forces for roughness perception in their daily lives. Our next challenge is to investigate how the pressing force and its active control can be related to the spatial spectrum of finger pad deformation in judging roughness.

V. Conclusions

A previous study investigated the link between the roughness perception of macroscopic surface features and the spatial spectrum of finger pad skin deformation [25]. To investigate this link further, we

estimated the roughness perception using a weighted linear combination of multiple spectral components, in contrast to a previous study that estimated the roughness perception using only individual spectral components. Close-up images of the finger pads were captured when the pads were statically pushed into the roughened specimens, and their Gabor filter outputs were computed to acquire the spatial spectra. The spectra were then linked to the subjective roughness values reported in the magnitude estimation task by using the PLS regression method. The weighted linear combination of spectral components exhibited good agreement with the roughness perception with a correlation coefficient of 0.82 ± 0.023, which is significantly higher than the correlation coefficient (0.75 ± 0.023) computed from the single spectral component. These results support the hypothesis that roughness perception is mediated by a linear combination of the outputs of multiple Gabor filter-like detectors for different spatial wavelengths. These findings can help us further understand the perceptual mechanisms of macroscopic roughness together with the existing literature on roughness perception.

REFERENCES

[1] W. M. Bergmann Tiest, "Tactual perception of material properties," *Vision Research*, vol. 50, no. 24, pp. 2775–2782, 2010.

[2] S. Okamoto, H. Nagano, and Y. Yamada, "Psychophysical dimensions of tactile perception of textures," *IEEE Transactions on Haptics*, vol. 6, no. 1, pp. 81–93, 2013.

[3] S. J. Bensmaïa, "Texture from touch," *Scholarpedia*, vol. 4, no. 8, p. 7956, 2009.

[4] K. Sathian, A. Goodwin, K. John, and I. Darian-Smith, "Perceived roughness of a grating: correlation with responses of mechanoreceptive afferents innervating the monkey's fingerpad," *Journal of Neuroscience*, vol. 9, no. 4, pp. 1273–1279, 1989.

[5] K. O. Johnson and S. S. Hsiao, "Evaluation of the relative roles of slowly and rapidly adapting afferent fibers in roughness perception," *Canadian Journal of Physiology and Pharmacology*, vol. 72, no. 5, pp. 488–497, 1994.

[6] J. R. Phillips, R. S. Johansson, and K. O. Johnson, "Representation of braille characters in human nerve fibres," *Experimental Brain Research*, vol. 81, no. 3, pp. 589–592, Aug 1990.

[7] R. S. Johansson and Åke B. Vallbo, "Tactile sensory coding in the glabrous skin of the human hand," *Trends in Neurosciences*, pp. 27–32, 1983.

[8] J. R. Phillips and K. O. Johnson, "Tactile spatial resolution. iii. a continuum mechanics model of skin predicting mechanoreceptor responses to bars, edges, and gratings," *Journal of neurophysiology*, vol. 46, no. 6, pp. 1204–1225, 1981.

[9] D. R. Lesniak and G. J. Gerling, "Predicting SA-I mechanoreceptor spike times with a skin-neuron model," *Mathematical Biosciences*, vol. 220, no. 1, pp. 15–23, 2009.

[10] K. O. Johnson, "The roles and functions of cutaneous mechanoreceptors," *Current Opinion in Neurobiology*, vol. 11, no. 4, pp. 455–461, 2001.

[11] D. T. Blake, S. S. Hsiao, and K. O. Johnson, "Neural coding mechanisms in tactile pattern recognition: the relative contributions of slowly and rapidly adapting mechanoreceptors to perceived roughness," *Journal of Neuroscience*, vol. 17, no. 19, pp. 7480–7489, 1997.

[12] S. J. Lederman, J. M. Loomis, and D. A. Williams, "The role of vibration in the tactual perception of roughness," *Perception & Psychophysics*, vol. 32, no. 2, pp. 109–116, 1982.

[13] S. J. Lederman and M. M. Taylor, "Fingertip force, surface geometry, and the perception of roughness by active touch," *Perception & Psychophysics*, vol. 12, no. 5, pp. 401–408, Sep 1972.

[14] T. Yoshioka, B. Gibb, A. K. Dorsch, S. S. Hsiao, and K. O. Johnson, "Neural coding mechanisms underlying perceived roughness of finely textured surfaces," *Journal of Neuroscience*, vol. 21, no. 17, pp. 6905–6916, 2001.

[15] M. A. Lawrence, R. Kitada, R. L. Klatzky, and S. J. Lederman, "Haptic roughness perception of linear gratings via bare finger or rigid probe," *Perception*, vol. 36, no. 4, pp. 547–557, 2007.

[16] A. Dépeault, E.-M. Meftah, and C. E. Chapman, "Tactile perception of roughness: raised-dot spacing, density and disposition," *Experimental brain research*, vol. 197, no. 3, pp. 235–244, 2009.

[17] K. Drewing, "Judged roughness as a function of groove frequency and groove width in 3d-printed gratings," in *International Conference on Human Haptic Sensing and Touch Enabled Computer Applications*. Springer, 2018, pp. 258–269.

[18] C. E. Connor and K. O. Johnson, "Neural coding of tactile texture: comparison of spatial and temporal mechanisms for roughness perception," *Journal of Neuroscience*, vol. 12, no. 9, pp. 3414–3426, 1992.

[19] G. A. Gescheider, S. J. Bolanowski, T. C. Greenfield, and K. E. Brunette, "Perception of the tactile texture of raised-dot patterns: A multidimensional analysis," *Somatosensory & Motor Research*, vol. 22, no. 3, pp. 127–140, 2005.

[20] J. Eck, A. L. Kaas, J. L. Mulders, L. Hausfeld, Z. Kourtzi, and R. Goebel, "The effect of task instruction on haptic texture processing: The neural underpinning of roughness and spatial density perception," *Cerebral Cortex*, vol. 26, no. 1, pp. 384–401, 2014.

[21] D. R. Lesniak, K. L. Marshall, S. A. Wellnitz, B. A. Jenkins, Y. Baba, M. N. Rasband, G. J. Gerling, and E. A. Lumpkin, "Computation identifies structural features that govern neuronal firing properties in slowly adapting touch receptors," *eLife*, vol. 3, p. e01488, 2014.

[22] H. P. Saal, B. P. Delhaye, B. C. Rayhaun, and S. J. Bensmaïa, "Simulating tactile signals from the whole hand with millisecond precision," *Proceedings of the National Academy of Sciences*, vol. 114, no. 28, pp. E5693–E5702, 2017.

[23] S. Kuroki, M. Sawayama, and S. Nishida, "The roles of lower-and higher-order surface statistics in tactile texture perception," *Journal of Neurophysiology*, 2021.

[24] M. Taylor and S. J. Lederman, "Tactile roughness of grooved surfaces: A model and the effect of friction," *Perception & Psychophysics*, vol. 17, no. 1, pp. 23–36, 1975.

[25] S. Okamoto and A. Oishi, "Relationship between spatial variations in static skin deformation and perceived roughness of macroscopic surfaces," *IEEE Transactions on Haptics*, vol. 13, no. 1, pp. 66–72, 2020.

[26] A. I. Weber, H. P. Saal, J. D. Lieber, J.-W. Cheng, L. R. Manfredi, J. F. Dammann, and S. J. Bensmaïa, "Spatial and temporal codes mediate the tactile perception of natural textures," *Proceedings of the National Academy of Sciences*, vol. 110, no. 42, pp. 17 107–17 112, 2013.

[27] J. D. Lieber, X. Xia, A. I. Weber, and S. J. Bensmaïa, "The neural code for tactile roughness in the somatosensory nerves," *Journal of Neurophysiology*, vol. 118, no. 6, pp. 3107–3117, 2017.

[28] C. Tymms, E. P. Gardner, and D. Zorin, "A quantitative perceptual model for tactile roughness," *ACM Transactions on Graphics*, vol. 37, no. 5, pp. 1–14, 2018.

[29] T. Lindeberg, "Normative theory of visual receptive fields," *Heliyon*, vol. 7, no. 1, p. e05897, 2021.

[30] A. Sutu, E.-M. Meftah, and C. E. Chapman, "Physical determinants of the shape of the psychophysical curve relating tactile roughness to raised-dot spacing: implications for neuronal coding of roughness," *Journal of Neurophysiology*, vol. 109, no. 5, pp. 1403–1415, 2013.

[31] S. J. Lederman, "Tactual roughness perception: spatial and temporal determinants." *Canadian Journal of Psychology*, vol. 37, no. 4, p. 498, 1983.

[32] C. E. Connor, S. S. Hsiao, J. R. Phillips, and K. O. Johnson, "Tactile roughness: neural codes that account for psychophysical magnitude estimates," *Journal of Neuroscience*, vol. 10, no. 12, pp. 3823–3836, 1990.

[33] S. J. Lederman, "Tactile roughness of grooved surfaces: The touching process and effects of macro-and microsurface structure," *Perception & Psychophysics*, vol. 16, no. 2, pp. 385–395, 1974.

[34] M. Hollins, F. Lorenz, and D. Harper, "Somatosensory coding of roughness: the effect of texture adaptation in direct and indirect touch," *Journal of Neuroscience*, vol. 26, no. 20, pp. 5582–5588, 2006.

[35] G. Corniani and H. P. Saal, "Tactile innervation densities across the whole body," *Journal of Neurophysiology*, vol. 124, no. 4, pp. 1229–1240, 2020.

[36] R. S. Johansson, "Tactile sensibility in the human hand: receptive field characteristics of mechanoreceptive units in the glabrous skin area." *Journal of Physiology*, vol. 281, no. 1, pp. 101–125, 1978.

[37] C. E. Chapman, F. Tremblay, W. Jiang, L. Belingard, and E.-M. Meftah, "Central neural mechanisms contributing to the perception of tactile roughness," *Behavioural Brain Research*, vol. 135, no. 1, pp. 225 – 233, 2002.

[38] R. M. Peters, E. Hackeman, and D. Goldreich, "Diminutive digits discern delicate details: Fingertip size and the sex difference in tactile spatial acuity," *Journal of Neuroscience*, vol. 29, no. 50, pp. 15 756–15 761, 2009.

[39] C. Tymms, D. Zorin, and E. P. Gardner, “Tactile perception of the roughness of 3d-printed textures,” *Journal of Neurophysiology*, vol. 119, no. 3, pp. 862–876, 2018.

Qingyu SUN received a B.S. degree in engineering from Tongji University, China in 2020 and has been a master’s student at Nagoya University, Japan, since 2020. His research interests include haptics and perception.

Shogo OKAMOTO received a B.S. degree in engineering from Kobe University in 2005 and M.S. and Ph.D. degrees in information sciences in 2007 and 2010, respectively, from the Graduate School of Information Sciences, Tohoku University. He was an assistant and associate professor in the Department of Mechanical Systems, Nagoya University till 2015 and 2021, respectively. Since 2021, he has been with the Department of Computer Sciences, Tokyo Metropolitan University, as an associate professor.

Yasuhiro AKIYAMA received his B.E. degree in engineering from Tokyo Institute of Technology, Tokyo, Japan in 2006, and his M.S. and Ph.D. degrees in engineering from the University of Tokyo, Tokyo in 2008 and 2011, respectively. Until 2016, he was an assistant professor at Nagoya University, Japan. Since 2022, he has been an associate professor in the Department of Mechanical Engineering and Mechatronics, Shinshu University, Japan. His main research interests include mechanical safety, human–robot interaction, and biomechanics.

Yoji YAMADA received his Ph.D. from the Tokyo Institute of Technology, Japan in 1990. He has been an associate professor at Toyota Technological Institute, Nagoya, Japan since 1983. In 2004, he joined AIST as the leader of the Safety Intelligence Research Group at the Intelligent Systems Research Institute. In 2008, he became a professor at the Graduate School of Engineering at Nagoya University. Since 2022, he has been the president of the National Institute of Technology, Toyota College.